Journal of Environment and Pollution

PRIME OPEN ACCESS

Volume 1, Issue 1

Research Article

Date of Submission: 01 Apr, 2025
Date of Acceptance: 02 June, 2025
Date of Publication: 12 June, 2025

Assessing Multi-Hazard Risk in Gulmidarbar Rural Municipality, Gulmi, Nepal

Sundar Tandan*, Basanta Raj Adhikari and Akhilesh Kumar Karna

Department of Civil Engineering, Pulchowk Campus, Institute of Engineering, Tribhuvan University, Nepal

***Corresponding Author:**
Sundar Tandan, Department of Civil Engineering, Pulchowk Campus, Institute of Engineering, Tribhuvan University, Nepal.

Citation: Tandan, S., Adhikari, B. R., Karna, A. K. (2025). Assessing Multi-Hazard Risk in Gulmidarbar Rural Municipality, Gulmi, Nepal. *J Environ Pollut, 1*(1), 01-12.

Abstract
The occurrences of different kinds of natural hazards in the Nepal Himalaya is increasing in recent years. The complex interaction between these hazards is poorly understood. The multi-hazard mapping underscores the pivotal role of hazard maps in disaster risk reduction, advocating for the creation of a multihazard map despite associated challenges in the Gulmidarbar Rural Municipality. The individual hazard maps for landslides, forest fire, flood and earthquakes were generated. Rigorous validation processes, including field verification, were done to ensure the accuracy of individual hazard maps before integration into the comprehensive multi-hazard map sing the Analytical Hierarchal Process (AHP). The vulnerability was calculated at lowest administrative levels incorporating physical and socio-economic factors. The multi-hazard map is prepared by combining the hazard and vulnerability at ward level. The analysis shows that Ward No.4 has high risk followed by Ward No.1. This analysis is important to the mayor and other policy makers in decision-making, emergency response, and urban planning, aiming to develop robust strategies that minimize losses and enhance resilience in the studied region.

Keywords: Landslide, Forest-Fire, Earthquake, Flood, Multi-Hazard, Risk, Vulnerability

Introduction
Nepal, situated in the seismic and seismically active Himalayan region, serves as a clear illustration of the intricate interactions among natural hazards that influence its topography [1]. Nepal encounters a range of natural hazards that destroy the country's-built environment and infrastructure, causing loss of life and property damage. Ongoing threats from natural hazards persistently jeopardize individuals, infrastructure, essential lifelines, and agricultural areas [2]. The most damaging natural hazards that cause lives and significant financial damage in Nepal include fires, earthquakes, landslides, lightning, and floods [3]. Most of the previous researchers are confirmed on the consequences of a single hazard, such as floods , earthquakes , forest fires, and landslides [4-7]. A risk assessment's primary objective is to determine the possibility that a" hazardous event," which is defined as a process that threatens both economic and human systems, will result in losses because of both individuals and financial resources [8]. So, the evaluation of risk and, consequently, the reduction of vulnerability involve employing multidisciplinary expertise in various interconnected physical and social processes to determine the overall level of risk associated with hazards [9].

Studies on the impacts of multi-hazards primarily focus on the individual effects of hazards such as landslides , forest fires , floods , and earthquakes [4-7]. Many places are prone to not only single hazards but also a combination of individual hazards. Therefore, studies on multi-hazard situations are necessary due to the combined effects of such types of hazards. Identifying areas prone to hazards and assessing the level of risk is crucial for developing preparedness, recovery, response, and mitigation strategies for both individual hazards and multi-hazard scenarios.

Multi-hazard mapping is important, although it is hampered by several issues, including a lack of comprehensive data, the challenge of integrating separate hazard maps, and the challenge of creating conditions and outcomes for hazards that are specific to a certain location [10-12].Decision-makers are thus prevented from identifying areas susceptible to many risks and putting precautions in place because many studies are restricted to a single natural hazard, differ in methodology, and cover a small research area [13]. Making a multi-hazard map has numerous advantages despite its many difficulties. Because the pre-disaster context can either emphasize or lessen the effects of an individual hazard, a multi-hazard strategy that considers the geographical, demographic, and physical contexts and their numerous linkages and feedbacks could significantly contribute to reducing human and financial losses [9].

Researchers have devised diverse methodologies to tackle the assessment of multihazard risks, implementing these strategies in various geographical settings [14]. Multi-hazard risk plays a crucial role in identifying highly susceptible zones and facilitating resource allocation for disaster preparedness, response, recovery, and mitigation strategies. This study analyses the four major hazards: landslides, forest fires, floods, and earthquakes that occur in the Gulmidarbar Rural Municipality. The allocation of weightage to each hazard during the creation of the multi-hazard map by AHP (Analytic Hierarchy Process) relies on input from local experts, surveys, and focal group discussions. This study conducts the multi-hazard assessment of the Gulmidarbar Rural Municipality. The multi-hazard risk map is created by integrating the multi-hazard map with the vulnerability map, which is derived from the weighting of both physical and social parameters.

Materials and Methods

Study Area

The Gulmidarbar Rural Municipality (Figure.1) is in the Gulmi district of Lumbini Province, Nepal. The geographic location of the rural municipality is 27° 55′ 14″ N 28° 07′ 00″ N to 83° 16′ 30″ E - 83° 22′ 45″ E with the total area of 79.99km^2. The municipality ranges in elevation from 623.755 to 2142.06 meters and experiences upper tropical, subtropical, and temperate climates. It has a population of 19,296 according to the 2078 census.

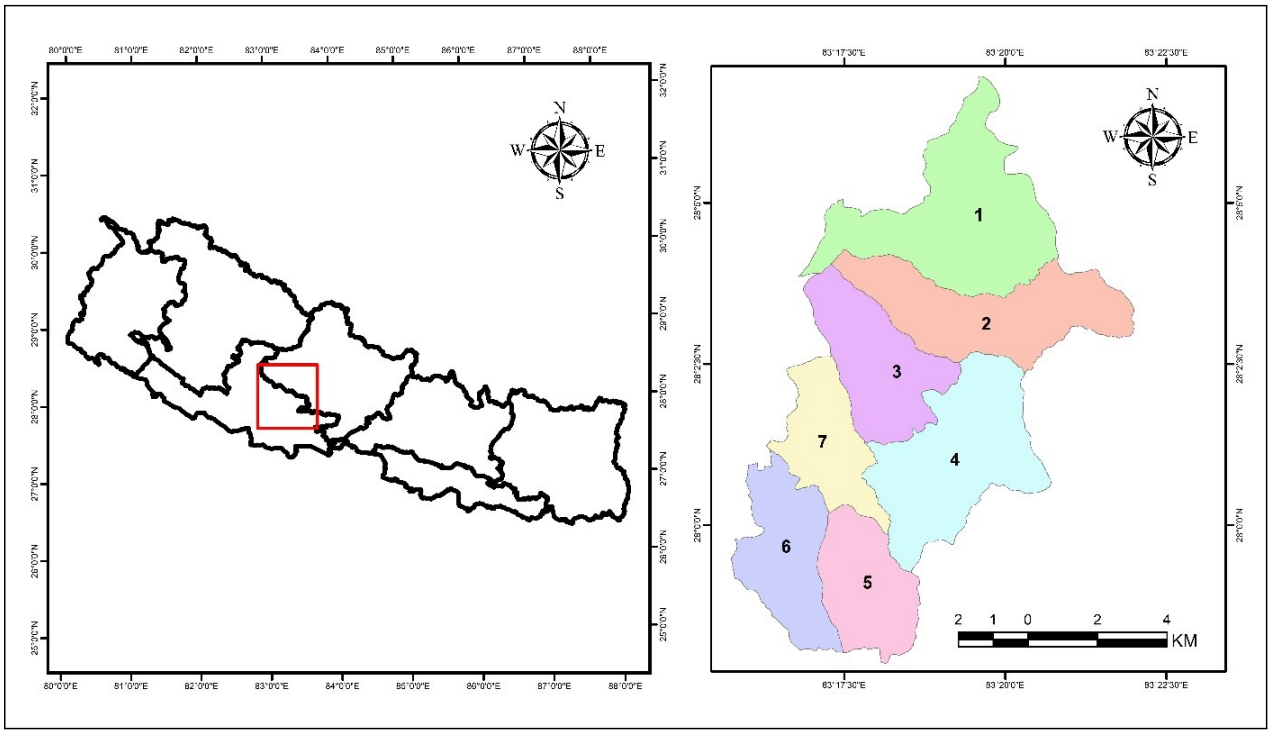

Figure 1: Location Map of Gulmidarbar Rural Municipality

Data Collection

Several sets of data were collected from various Nepal Government Organizations and International Government Organizations, including the Digital Elevation Model (DEM), hydrology of the study area, which includes the rainfall, river discharge, geology map of Nepal produced by International Centre for Integrated Mountain Development (ICIMOD,2021), land use map (30 m resolution) prepared by ICIMOD (2019), vegetation index data (NDVI), distance to road, distance to stream, landcover, relative relief, lithology, soil, and seismic zoning map of Nepal. The type and the sources of data are summarized in (Table 1).

Individual Hazard Mapping

Earthquake Hazard Mapping

Probabilistic seismic hazard assessment considers uncertainties about the magnitude, position, and timing of earthquakes [15].The earthquake (seismic) zoning map of the

Datasets	Source	References
DEM	ALOS Palsar	[16]
Slope, Aspect, Elevation, TWI, Relative Relief, Curvature	DEM	[16]
Landuse/Landcover (2019), Soil Data & Geology	ICIMOD	[17]
Distance to Drainage, Road	Government Website	[18]
Meterological and Hydrological Data	DHM	[19]
Sentinel 2 Images (NDVI/NDMI)	European Satellite Agency	[16]
Wind Velocity	Global Wind Atlas	[20]
Settlement Data	World Settlement (R26,C26)	[21]
Fire Data (20 Years)	NASA Firms	[22]
Landslide Inventory	Google Earth Pro/Field Visit	[23]
Vulnerability Data	(Census,2078), Survey	[24]

Table 1: Table Showing Datasets and its Sources

Study area was created using the seismic map created by NBC:2020. Using georeferencing, the seismic zoning map image file was imported into QGIS and transformed into a georeferenced image. To get the seismic zoning map of the study area, the georeferenced image was cropped by the study area and the clipped file was classed using the NBC:2020.

Flood Hazard Mapping

The technique and outcome capabilities of flood hazard mapping have greatly improved, enabling policymakers to precisely expect and identify regions that are vulnerable to flooding [25].The following factors affect the flood are: Landcover: Wetlands, pavement, and other impermeable surfaces can decrease the amount of rainfall that reaches the ground and increase surface runoff , Discharge: The stream's overflowing discharge widens its channel by overflowing its banks and inundating the nearby low-lying areas , Rainfall: An increase in rainfall increases the water's capacity to absorb, resulting in a flood caused by the rainfall , Inundation Depth: The intensity of flooding increases as the inundation depth rises [26-28].

The flood hazards map in this study employed the Rain-on-grid method, combining QGIS spatial analysis and HEC-RAS modeling. Using RAS-MAPPER projection, DEM, landcover, and Manning's coefficient were integrated to create a 2D flow area with 100*100 m mesh size. Inlet and outlet boundaries were set based on rainfall data. The model incorporated meteorological stations and daily rainfall for unsteady flow analysis, validated against observed discharge. Post-validation, rainfall for a 100-year return period was calculated, and the inundation depth was classified in QGIS.

Forest Fire Susceptibility Mapping

Globally, the number of forest fires is increasing, with Asia accounting for most of the significant incidents [12]. Based on a survey of the literature, Frequency Ratio method was used for the susceptibility mapping of the study area.

Landslide Susceptibility Mapping

It is a possibility that a landslide may happen in a specific location because of the local terrain. Numerous important geological, topographical, and other factors are selected and linked both separately and collectively to the occurrence of landslides. The following are the factors that influence landslides and forest fires based on the literature review:

- **Inventory:** The prior reports, aerial photo interpretation, and several kinds of field surveys were used to construct the inventory map. A total of 25 inventory landslides were documented throughout the last 15 years, using Google Earth Pro to produce the landslide inventory for this study. 20-year point data of forest fire inventory was obtained from the MODIS Data and converted into raster data for analysis.
- **Aspect:** Soil moisture, vegetation cover, and soil thickness are among the additional variables that indirectly affect the aspect (slope orientation), which also affects exposure to wind, sunlight, and precipitation [29]. The study area's aspect map was created using DEM data and was categorized into nine classes: East (67.5°-112.5°), South-East (112.5°-157.5°), South (157.5°-202.5°), South-West (202.5°-247.5°), West (247.5°-292.5°), North (0°-22.5° and 337.5°-360°), and North East (22.5°-67.5°) (Figure 2).
- **Slope:** In addition to meteorological events like rainfall and sunlight levels, drying winds, and the area's morphological structure, slope affects hydrological activities like evapotranspiration, weathering, vegetation, and plant root growth that contribute to the various hazards (landslides, forest fires, and floods) [30]. DEM data were used to prepare the research area's map's slope. The slope was divided into five classes: 0–15°, 15–30°, 30–50°, 50–70°, and 70–90°(Figure 2).
- **Land Use and Landcover:** Several land use and cover changes increase the number of unstable slopes (i.e., promote the propensity for various hazards occurrence) and can have a significant impact on them (e.g., deforestation, slope ruptures to road construction, steep slopes) [31]. After being resampled from 30 m resolution to 12.5 m resolution,

the land use map created by ICIMOD was utilized in this investigation (Figure 2).

- **Curvature:** Curvature affects the driving and resistive forces in the mass flow direction. Three classifications were identified in the curvature map which was produced using the DEM: convex (positive), flat (zero), and concave (negative) (Figure 2).
- **Distance from Drainage and Road:** Since the distance to settlement erodes the slope base and saturates the underwater portion of the slope-forming material, rivers with multiple drainage networks are more likely to experience landslides and floods [32]. The buffer tool in QGIS was utilized to create the stream map, which was categorized into four subclasses: 50-<150, 150-<500, and >500 m (Figure 2).

Depending on its position in the environment, a road segment may function as a barrier, a net source, a net sink, or a corridor for water movement; hence, it is usually a source of dangers [33]. The QUickOSM plugin was utilized to extract the road layer from OpenStreetMap. The buffer tool was employed to develop the distance from the road, which was then categorized into three subclasses: <300, 300-<500, and >500 m (Figure 2).

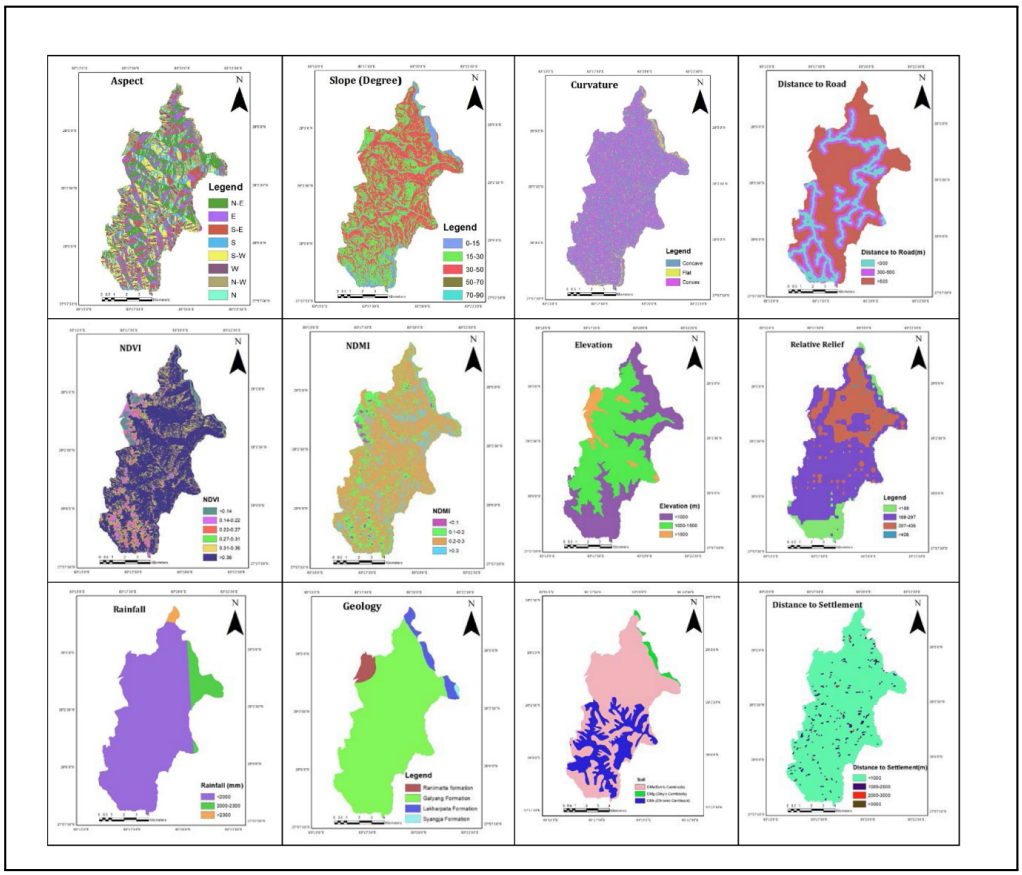

Figure 2: Thematic Maps of Factors Used in Study

NDVI and NDMI

Since natural hazards are linked to human involvement on hill slopes, vegetation cover frequently has a significant impact on their occurrence [34]. The Landsat-8 satellite image was converted into an NDVI using the following formula: NDVI=(NIR-R)/(NIR+R), where NIR stands for near-infrared band spectral reflectance and R for red band spectral reflectance. Subclasses:<0.14,0.14<0.22,0.22-<0.27,0.27-<0.31,0.31-<0.36, and>0.36 were used to classify it (Figure2).

A vegetation index that is frequently used to determine the moisture content of vegetation is the Normalized Difference Moisture Index, or NDMI. The following formula was used to produce it from the Landsat-8 satellite: NDMI = (NIR - MIR) / (NIR + MIR), where NIR is the near-infrared band (Band 8A) reflectance value and MIR is the mid-infrared band (Band 11) reflectance value. The following subclasses were assigned to it: <0.1,0.1-<0.2,0.2<0.3, and >0.3 (Figure 2).

Elevation and Relative Relief

Elevation is thought to be one of the elements influencing natural hazards because it influences environmental parameters such as vegetation, temperature, precipitation, and humidity [35]. The elevation map was created using DEM and categorized as : <1000, 1000-<1500, and >1500 m (Figure 2). Maps displaying relative relief show the potential energy for mass movement and erosion resulting from variations in elevation within a unit area. The classifications assigned to it were <188, 188-<297, 297-<406, and >406.

Rainfall

Although there are risks associated with rainfall, ground conditions are also important [36]. The study area's rainfall was classified as Fig 2f: <2000, 2000<2300, and >2300 mm based on the interpolation using the Thiessen polygon utilizing the stations Tamghas (725), Bharse (733), Musikot (722), and Ridi (701).

Geology and Soil

Geology affects hazards as it determines the permeability of the soil and the strength of the rock in a certain place. The ICIMOD (2020) geological map was used. In the study region, formations such as Lakharpata, Galyang, Syangja, and Ranimatta were found (Figure 2).

Three types of soil data were identified: CMe (Eutric Cambisols), CMg (Gleyic Cambisols), and CMx (Chromic Cambisols) (Figure 2). The soil data was received from the ICIMOD.

Distance to Settlement

Most urban poor people live in informal settlements, which are usually located close to dangerous natural areas. Data on settlement was acquired from NASA companies (R_{26},C_{26}). The buffer tool provided the distance to the settlement map, which was classified as: 1000-<2000, 2000-<3000, and >3000 m (Figure 2).

Wind Speed

Wind promotes the spread of fires by directing the flames towards unburned fuels in front of the fire and transferring heat and embers to new fuels. The global wind atlas provided the wind speed data, which was categorized: <1,1<1.6,1.6-<2.4,2.4-<3.2 and >3.2 m/sec (Figure 2).

Due to its ease of use, data accessibility, geographical analysis, comparative analysis, and interpretability, the frequency ratio approach was used in this study for the mapping of the susceptibility to landslides and forest fires. Based on the literature review, a total of ten and eleven influencing factors were employed for the mapping of the susceptibility to landslides and forest fires, respectively.

Multi-Hazard Risk Assessment

The individual hazard maps were verified and normalized using the raster calculator [9]. The validation individual hazards map was normalized by using the equation;

$$H_{\text{new}} = \frac{H - H_{\min}}{H_{\max} - H_{\min}} \qquad (1)$$

Where:
H_{new} is the normalized value of the hazard map, H is the original value of the hazard map,
H_{min} is the minimum value of the hazard map, and H_{max} is the maximum value of the hazard map.

Saaty has developed a systematic method for applying AHP to decision-makingrelated research [37]. The method starts with (i) describing the issue and establishing the goal and objective; (ii) putting the objectives at the top of the hierarchy, then the intermediate levels; and (iii) organizing the objectives at the bottom level, which usually has the list of alternatives. (iii) allocating numerical values according to the proportionate weight of each factor (pairwise comparison); (iv) creating the comparison matrix; and (v) computing the normalized principal eigenvectors, which incorporate the parameter weights. On a scale of 1 to 9, where 1 represents equal relevance and 9 represents the exceptional importance of one domain over another, experts rank the important levels. Every pairwise comparison immediately assigns a reciprocal. The maximum eigenvalue, consistency ratio, consistency index, and normalized primary eigenvectors are calculated for each criterion. For obtaining the consistency index (CI) the maximum eigenvalue (λ_{max}) is used as given by the equation:

$$CI = \frac{(\lambda_{max} - n)}{(n-1)} \qquad (2)$$

Where n is the size of the matrix. For the AHP method, the consistency ratio (CR) which is determined by the equation below should be valid only when CR is less than 10 percent, otherwise, the matric is inconsistent and judgment should be modified to validate the realistic results [38].

$$CR = \frac{CI}{RI} \qquad (3)$$

Where RI is the random consistency index for various matrix orders (n).

Hazards	Landslide (H1)	Forest Fire (H2)	Flood (H3)	Earthquake (H4)	Weight (Wi)
Landslide (H1)	1.00	4.00	3.00	6.00	0.549
Forest Fire (H2)	0.25	1.00	0.50	3.00	0.147
Flood (H3)	0.33	2.00	1.00	4.00	0.239
Earthquake (H4)	0.17	0.33	0.25	1.00	0.065

Table 2: Table Showing the Calculation of the Weight of Each Hazard

The weight of each hazard was calculated based on the survey among the chairperson of the seven wards, engineer and chairperson of Gulmidarbar Rural Municipality. The landslide has the highest weightage and the earthquake has lowest. The earthquake hazard weightage was not according to the peak ground acceleration value but rather based on the information collected from the survey among the local experts.

Number of Hazards (n)	max	Random Index (RI)	Consistency Index (CI)	Consistency Ratio (CR)
4.000	4.081	0.900	0.027	0.030

Table 3: Table Demonstrating Pairwise Comparative Consistency

The following calculation was used to generate the multihazard map based on the weightage value [13]:

$$MHI = \sum_{i=1}^{n} H_i \times W_i \qquad (4)$$

Where MHI is the multi-hazard index, n is the number of hazards, hi is individual hazards and Wi is the weightage of each hazard from the AHP method.

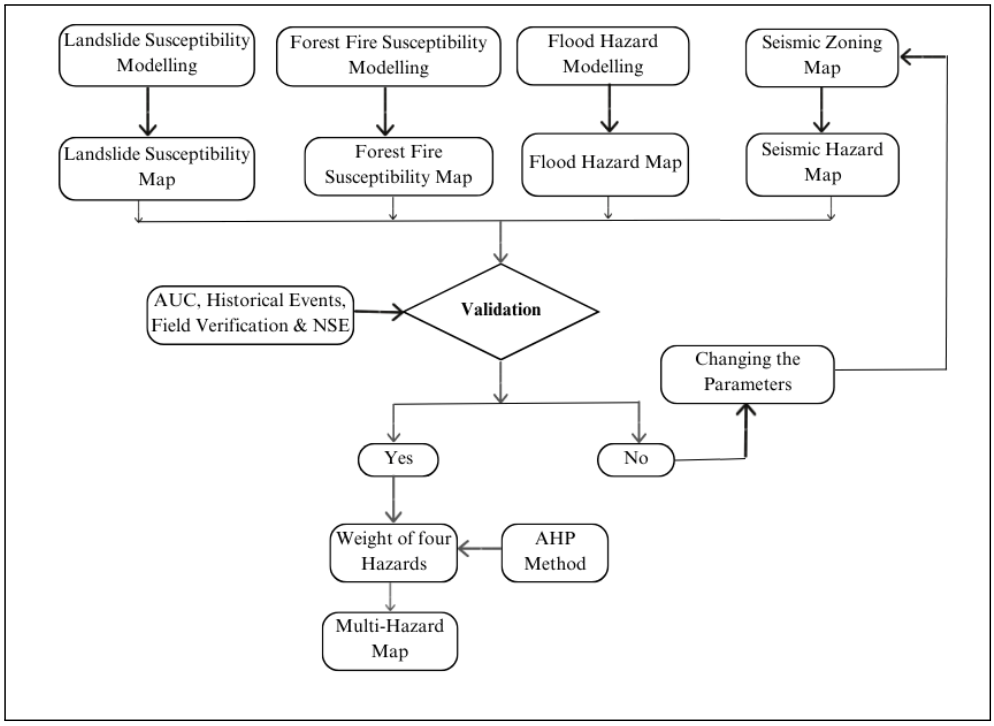

Figure 3: Methodology for Preparation of Multi-Hazard Susceptibility Map

The ward-specific vulnerability index was computed using physical and social parameters.

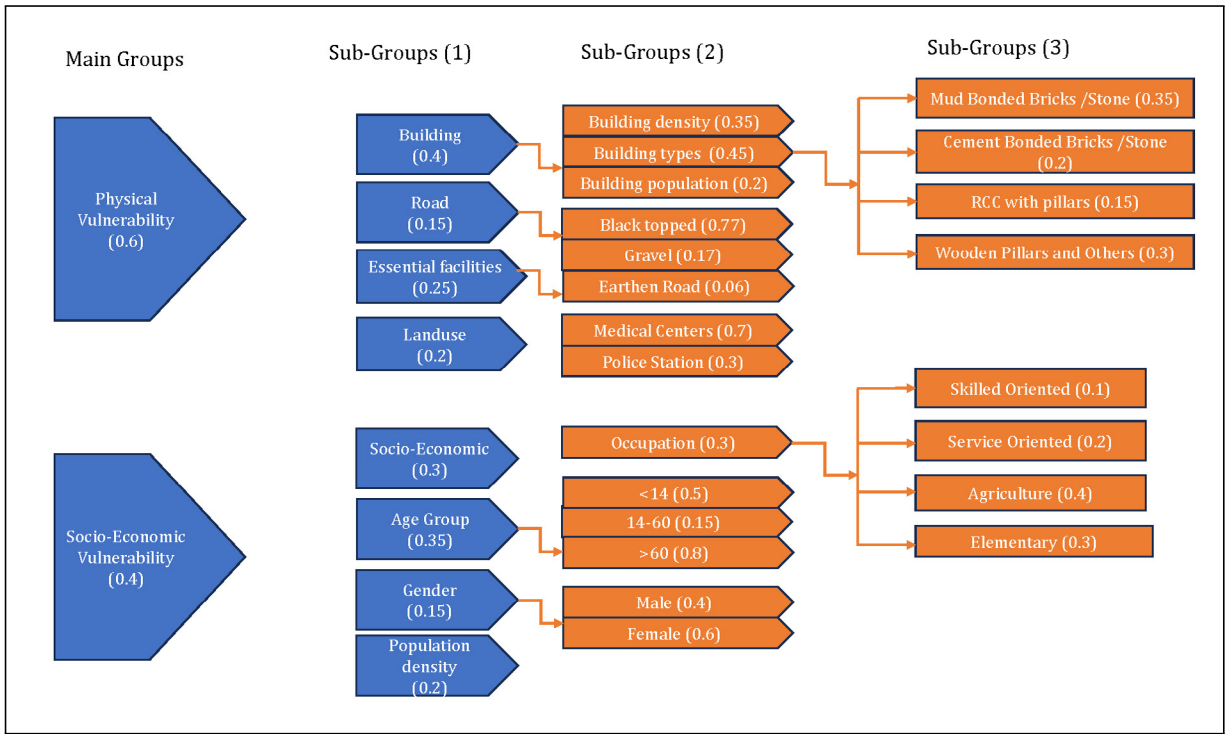

Figure 4: Methodology for Preparation of Multi-Hazard Susceptibility Map

Weightings for each parameter were determined through expert judgments, literature paper, interviews, focus group discussions, and surveys across different wards in the rural municipality. Physical vulnerability included buildings, roads, essential facilities, and land use, while social vulnerability considered socio-economic factors, age groups, gender, and population density. The total vulnerability [39] was calculated by the sum of the physical and the social vulnerability. The vulnerability map and the multi-hazard map were combined to obtain the multi-hazard risk map of the study area given by the equation [40]:

$$Risk = Hazard \times Vulnerability \qquad (5)$$

Results and Discussions

Individual Hazard Zonation

Landslide Susceptibility Assessment

To identify the various degrees of susceptibility to landslide occurrence, ten thematic layers total, with the following weights assigned: aspect (8%), slope (12%), geology (9%), land use (11%), curvature (9%), distance from drainage (8%), distance from the road (9%), rainfall (11%), Normalized Difference Vegetation Index (12%), and relative relief (11%) were calculated from the heuristic method. The landslide susceptibility map was divided into five categories using the Natural Jenks classification method. The landslide susceptibility map (Figure) shows that 11.07% of the area was very low susceptible to landslides, 1883% low susceptible, 28.17% medium, 22.17% high, and 19.89% very high susceptible to landslides (Table 4).

Forest Fire Susceptibility Assessment

For the forest fire susceptibility map in the study area, eleven thematic layers and their corresponding weights were calculated using the Frequency Ratio (FR) method, with the following weights: aspect (6%), slope (11%), topographic wetness index (9%), curvature (8%), soil (13%), distance from road (6%), distance from settlement (16%), NDVI (6%), NDMI (8%), elevation (12%), and wind speed (5%). The distance from the settlement exerted the most significant influence on weight, whereas wind speed had the least impact Using the Jenks breaks method, the forest fire susceptibility map has been classified into five classes: very low, low, medium, high, and very high. The forest fire susceptibility map Figure 5) indicates values of 6.22% very low,26.76% low, 32.96% medium, 29.71% high, and 4.36% very-high hazard zones (Table 4).

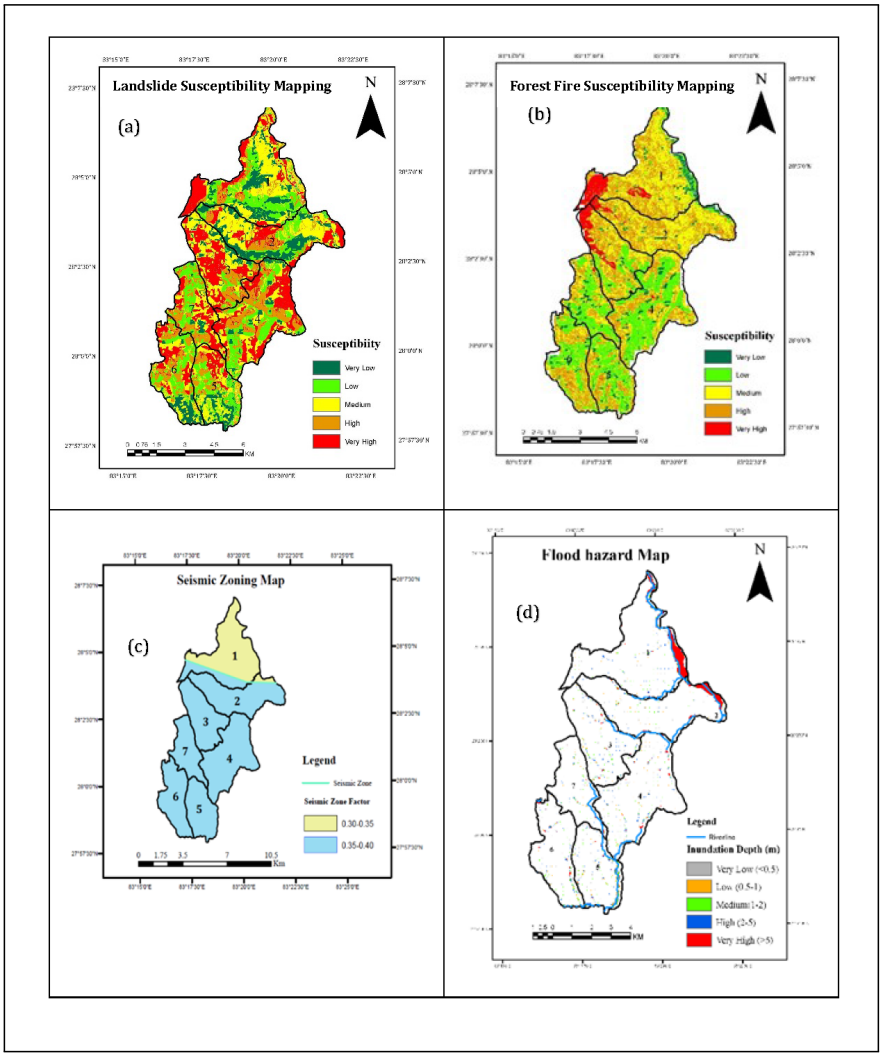

Figure 5: Individual Hazard Assessment (a) Landslide Susceptibility Mapping; (B) Forest Fire Susceptibility Mapping; (c) Seismic Zoning Map; (D) Flood Hazard Map

Seismic Zoning Map

From the seismic zoning map of Nepal, the seismic zoning map of the study area was created. Based on the seismic zones (NBC:2020), the seismic zoning map was divided into four classes: 0-0.25, 0.25-0.3, 0.3-0.35, and 0.35-0.40. The (Figure 5) indicates that 81.57% of the land's surface is found at the seismic zone factor 0.35-0.40, whereas 18.43% is located at the seismic zone factor 0.30-0.35.

Flood Hazard Assessment

From the HEC-RAS 2D flood hazard map was created using the rain-on-grid technique for a 100-year rainfall return period. Based on the depth of inundation, the flood hazard map was divided into five groups (Figure 5): very low (<0.5), low (0.5-<1), medium (1-<2), high (2-<5), and very high (>5) levels. From the overall area of 0.52%-very low, 0.57% low,0.82% medium, 1.24% high, and 2.60% very-high hazard zones (Table 4) [41].

Validiation of the Individual Hazard Maps

During the inventory map compilation process at Google Earth Pro, a field visit was undertaken and the Area under Curve (AUC) method was utilized to validate

Hazard Zonation	Landslide (%)	Forest Fire (%)	Flood (%)	Multi-hazard (%)
Very Low	11.07	6.22	0.52	12.04
Low	18.83	26.76	0.57	27.53
Medium	28.17	32.96	0.82	28.12
High	22.17	29.71	1.24	20.69
Very High	19.89	4.36	2.6	11.63

Table 4: Hazard Zonation Percentage Area of Landslide, Forest Fire, Flood, and Multi-Hazard in Gulmidarbar Rural Municipality

The landslide hazard map. Based on the Area Under Curve (AUC) for the landslide susceptibility map, the success and prediction rates were found to be 71.4% and 65.8%, respectively. The area under the curve (AUC) approach was used to validate the forest fire hazard map. It was found that the model's success and prediction rates were, respectively, 73.8% and 66.2%. Nepal Building Code:2020 provided the seismic zoning map that was used.

The flood hazards map was calibrated for year (2000) and the calibrated parameters was used for the model validation (2018) using the discharge data for several years using the following statistical indicators (Table 5): PBIAS, Coefficient of determination (R2), Nash-Sutcliffe efficiency (NSE) [42].

S.N.	Indicators	Calibration (2000)	Goodness of fit	Validation (2018)
1	NSE	0.648	Good	0.624
2	PBIAS (%)	2.794	Very Good	0.408
3	R2	0.919	Very Good	0.938

Table 5: Stastical Indicators Obtained from Flood Hazard Map Calibration and Validation

Multi-Hazard Susceptibility Assessment

After each susceptibility map were validated and normalized, the individual hazards (floods, landslides, fires, and earthquakes) map were integrated and created as a multi-hazard map using the Analytical Hierarchy Process (AHP). Using Jenks Natural breaks classification, the multi-hazard map was divided into five classes: very low, low, medium, high, and very high. The multi-hazard map Figure 6 shows that there are hazard zones totaling 12.04% very low, 27.53% low, 28.12% medium, 20.69% high, and 11.63% very high (Table 4).

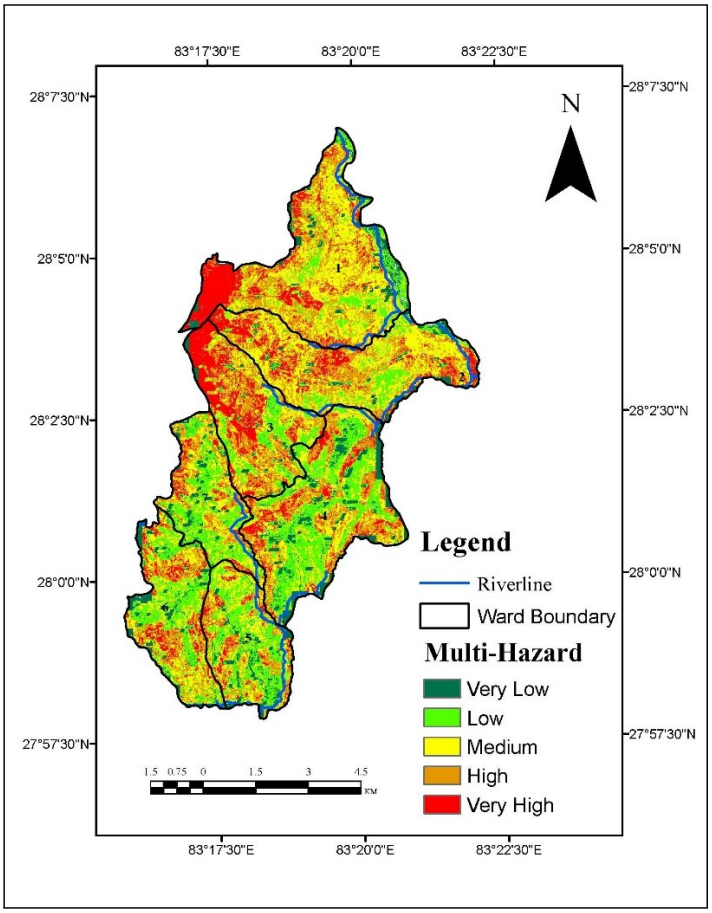

Figure 6: Multi-Hazard Susceptibility Map of Study Area

Vulnerability Index

The score for each of the parameters was calculated based on the weightage determined by the surveys, literature review, and local experts. The physical vulnerability index (Table 6) and the social vulnerability index (Table 6) were added to develop the complete vulnerability map. From the (Table 6) it was seen that Ward No. 4 emerged as the most vulnerable due to insufficient facilities, notably the absence of a police station, and a substantial portion of the cultivation area located within. Social vulnerability analysis indicated a higher proportion of individuals aged <14 and >60 in this ward. In contrast, Ward No. 3 exhibited lower vulnerability attributed to enhanced infrastructure, the existence of a health post, and a well-paved road.

Ward No	Physical Vulnerability Index	Social Vulnerability Index	Total Vulnerability Index
1	0.62	0.50	0.57
2	0.62	0.34	0.51
3	0.52	0.10	0.35
4	0.88	0.65	0.79
5	0.60	0.09	0.40
6	0.58	0.09	0.39
7	0.82	0.17	0.56

Table 6: Table Showing Vulnerability Indexes of Each Wards

Multi-Hazard Risk Assessment

Using the raster calculator in QGIS, the multi-hazard risk map was created by multiplying the multi-hazard and total vulnerability values. The multi-hazard risk map was classified using the Jenks natural breaks (George Frederick Jenks) classification method in QGIS into five classes: very low, low, medium, high, and very-high. The (Figure 7) shows the multi-hazard risk map of the study area:

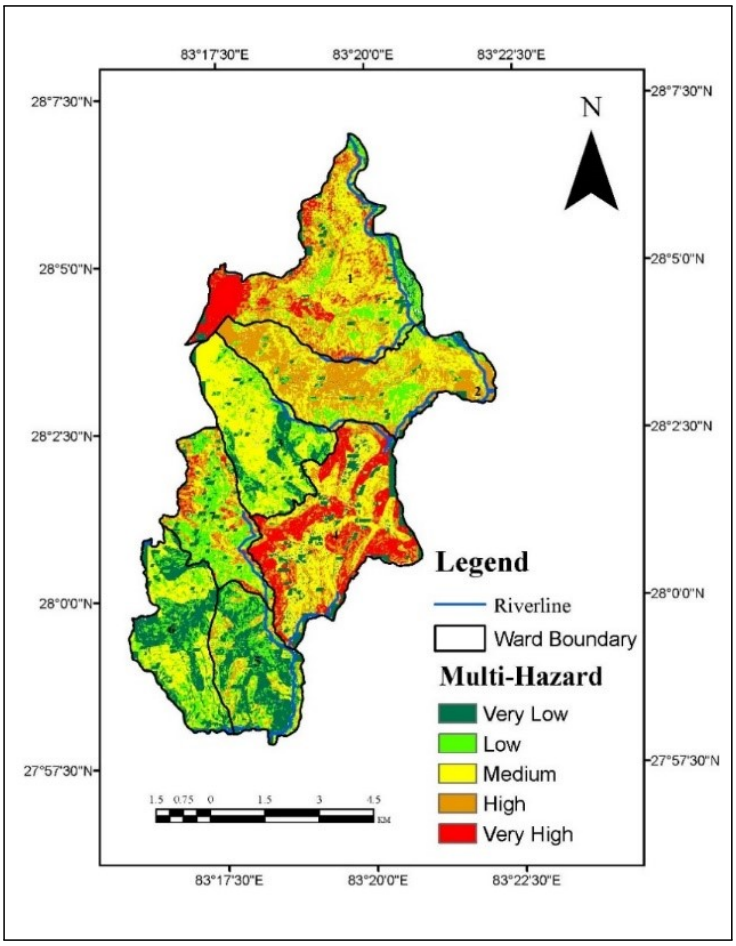

Figure 7: Multi-Hazard Risk Map of Study Area

From the multi-hazard risk map 19.58% of the total area was at very low, 25.86% low, 28.63% medium, 15.10% high and 10.83% at very high-risk zones (Table 7).

S. No.	Multi-Hazard Risk Level	Area (sq. km)	Percent
1	Very Low	15.59	19.58%
2	Low	20.58	25.86%
3	Medium	22.79	28.63%
4	High	12.01	15.10%
5	Very High	8.63	10.83%

Table 7: Table Showing Multi-Hazard Risk Level for Different Levels

The (Figure 8) illustrates the ward-wise multi-hazard, risk, and vulnerability map shown that Ward No.04 was at high risk due to the high number of the landslides, lack of essential facilities like a police station, higher population density and with a significant partition of the cultivation area. Similarly, Ward No.03 was at low risk due to the lesser number of the landslides, improved infrastructure, presence of the health post and a black -topped road.

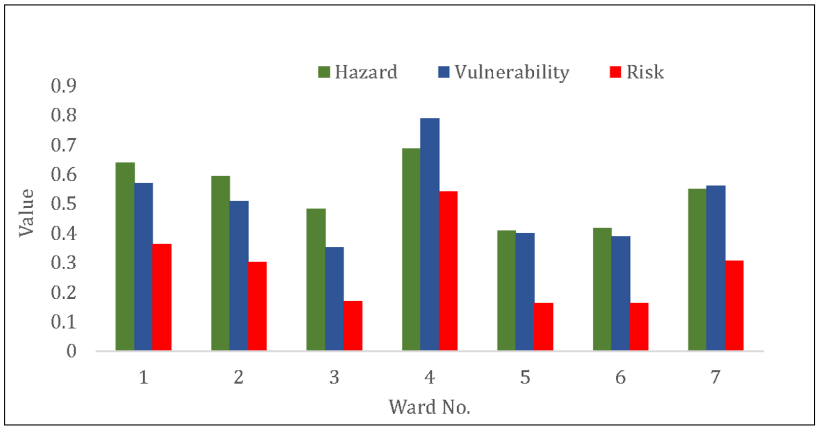

Figure 8: Comaparison of Hazard, Vulnerability Risk at Ward-Wise

Conclusion

The preparation of multi-hazard map is a data driven method where this study considered four hazards: earthquake, forest fire, floods, and landslides. This study employed frequency ratio for the preparation of landslides and forest fire susceptibility maps, rain-on-grid for flood hazard maps, and seismic zoning map of Nepal was used for seismic zoning map. A key focus was the integration of individual hazard maps using the Analytic Hierarchy Process (AHP) to assess and manage overall risk in the rural municipality.

The study area is mainly in a medium susceptibility zone to multi-hazards (28.12%), followed by low susceptibility (27.53%), high susceptibility (20.69%), very low susceptibility (12.04%), and very high susceptibility (11.63%). The Ward No.4 is at highly vulnerable and Ward No.3 is at less vulnerable among the seven wards. This study assists planners, rescue workers, policymakers, and decision-makers in devising more effective strategies by efficiently allocating resources. Additionally, the results from this map aid in identifying locations vulnerable to both single and multiple hazards.

Acknowledgement(s)

The authors express gratitude to Gulmidarbar Rural Municipality, Pulchowk Campus faculty for guidance and fostering an enriching research environment.

Disclosure statement

Research maintains objectivity, honesty, and impartiality, free from financial conflicts.

Funding

The research is self-funded, independent financial support.

References

1. Mukherji, A., Sinisalo, A., Nüsser, M., Garrard, R., & Eriksson, M. (2019). Contributions of the cryosphere to mountain communities in the Hindu Kush Himalaya: a review. Regional Environmental Change, 19, 1311-1326.
2. Aksha, S. K., Juran, L., & Resler, L. M. (2018). Spatial and temporal analysis of natural hazard mortality in Nepal. Environmental Hazards, 17(2), 163-179.
3. Gautam, D., Thapa, S., Pokhrel, S., & Lamichhane, S. (2021). Local level multi-hazard zonation of Nepal. Geomatics, Natural Hazards and Risk, 12(1), 405-423.
4. Kabenge, M., Elaru, J., Wang, H., & Li, F. (2017). Characterizing flood hazard risk in data-scarce areas, using a remote sensing and GIS-based flood hazard index. Natural hazards, 89, 1369-1387.
5. Dhar, S., Rai, A. K., & Nayak, P. (2017). Estimation of seismic hazard in Odisha by remote sensing and GIS techniques. Natural hazards, 86, 695-709.
6. Adab, H., Kanniah, K. D., & Solaimani, K. (2013). Modeling forest fire risk in the northeast of Iran using remote sensing and GIS techniques. Natural hazards, 65, 1723-1743.
7. Pellicani, R., Argentiero, I., & Spilotro, G. (2017). GIS-based predictive models for regional-scale landslide susceptibility assessment and risk mapping along road corridors. Geomatics, Natural Hazards and Risk, 8(2), 1012-1033.
8. Wohl, E. E. (2011). Anthropogenic impacts on flood hazards.
9. Aksha, S. K., Resler, L. M., Juran, L., & Carstensen Jr, L. W. (2020). A geospatial analysis of multi-hazard risk in Dharan, Nepal. Geomatics, Natural Hazards and Risk, 11(1), 88-111.

10. Gallina, V., Torresan, S., Critto, A., Sperotto, A., Glade, T., & Marcomini, A. (2016). A review of multi-risk methodologies for natural hazards: Consequences and challenges for a climate change impact assessment. Journal of environmental management, 168, 123-132.
11. Tate, E., Cutter, S. L., & Berry, M. (2010). Integrated multihazard mapping. Environment and Planning B: Planning and Design, 37(4), 646-663.
12. Johnson, K., Depietri, Y., & Breil, M. (2016). Multi-hazard risk assessment of two Hong Kong districts. International Journal of Disaster Risk Reduction, 19, 311-323.
13. Khatakho, R., Gautam, D., Aryal, K. R., Pandey, V. P., Rupakhety, R., Lamichhane, S., ... & Adhikari, R. (2021). Multi-hazard risk assessment of Kathmandu Valley, Nepal. Sustainability, 13(10), 5369.
14. Pourghasemi, H. R., Kariminejad, N., Amiri, M., Edalat, M., Zarafshar, M., Blaschke, T., & Cerda, A. (2020). Assessing and mapping multi-hazard risk susceptibility using a machine learning technique. Scientific reports, 10(1), 3203.
15. Chaulagain, H., Rodrigues, H., Silva, V., Spacone, E., & Varum, H. (2015). Seismic risk assessment and hazard mapping in Nepal. Natural Hazards, 78, 583-602.
16. (USGS), (2020). U.S.G.S.: Earth Explorer Data Available on the World Wide Web. Accessed: 2021-05-10.
17. FRTC: (2022). Land cover of Nepal [Data set]. [Online; accessed 20-November-2023].
18. Google Maps: (2020). Gulmi District. Accessed: 2021-11-12 .
19. Department of Hydrology and Meteorology (DHM): (2021). Hydrological and Meteorological Records of Nepal. Government of Nepal, Ministry of Water Resources, Department of Hydrology and Meteorology, Kathmandu, Nepal
20. Global Wind Atlas: (2023). Global Wind Atlas. Accessed: 2023-04-01.
21. Google Earth Engine Community: (2022). World Settlement Footprint (WSF). Accessed: 2022-08-02.
22. NASA Fire Information for Resource Management System (FIRMS): (2022). NASA FIRMS. Accessed: 2022-04-12 .
23. Google Earth Pro: (2023). Google Earth Pro. Version 7.3.3.
24. National Population and Housing Census 2021 (National Report)
25. Mudashiru, R. B., Sabtu, N., Abustan, I., & Balogun, W. (2021). Flood hazard mapping methods: A review. Journal of hydrology, 603, 126846.
26. Idowu, D., & Zhou, W. (2021). Land use and land cover change assessment in the context of flood hazard in Lagos State, Nigeria. Water, 13(8), 1105.
27. Sarchani, S., Seiradakis, K., Coulibaly, P., & Tsanis, I. (2020). Flood inundation mapping in an ungauged basin. Water, 12(6), 1532.
28. de MOEL, H., & Aerts, J. C. J. H. (2011). Effect of uncertainty in land use, damage models and inundation depth on flood damage estimates. Natural Hazards, 58, 407-425.
29. Clerici, A., Perego, S., Tellini, C., & Vescovi, P. (2006). A GIS-based automated procedure for landslide susceptibility mapping by the conditional analysis method: the Baganza valley case study (Italian Northern Apennines). Environmental Geology, 50, 941-961.
30. Galli, M., Ardizzone, F., Cardinali, M., Guzzetti, F., & Reichenbach, P. (2008). Comparing landslide inventory maps. Geomorphology, 94(3-4), 268-289.
31. Reichenbach, P., Busca, C., Mondini, A. C., & Rossi, M. (2014). The influence of land use change on landslide susceptibility zonation: the Briga catchment test site (Messina, Italy). Environmental management, 54, 1372-1384.
32. Akgün, A., & Türk, N. (2011). Mapping erosion susceptibility by a multivariate statistical method: a case study from the Ayvalık region, NW Turkey. Computers & geosciences, 37(9), 1515-1524.
33. Pradhan, B., & Lee, S. (2010). Landslide susceptibility assessment and factor effect analysis: backpropagation artificial neural networks and their comparison with frequency ratio and bivariate logistic regression modelling. Environmental Modelling & Software, 25(6), 747-759.
34. Pradhan, B., & Lee, S. (2009). Landslide risk analysis using artificial neural network model focusing on different training sites. Int J Phys Sci, 3(11), 1-15.
35. Dou, J., Yamagishi, H., Pourghasemi, H. R., Yunus, A. P., Song, X., Xu, Y., & Zhu, Z. (2015). An integrated artificial neural network model for the landslide susceptibility assessment of Osado Island, Japan. Natural Hazards, 78, 1749-1776.
36. Kim, J., Kim, Y., Jeong, S., & Hong, M. (2017). Rainfall-induced landslides by deficit field matric suction in unsaturated soil slopes. Environmental Earth Sciences, 76, 1-17.
37. Saaty, T. L. (1980). The analytic hierarchy process (AHP). The Journal of the Operational Research Society, 41(11), 1073-1076.
38. Saaty, T. L., & Vargas, L. G. (2012). Models, methods, concepts & applications of the analytic hierarchy process (Vol. 175). Springer Science & Business Media.
39. Guillard-Gonçalves, C., & Zêzere, J. L. (2018). Combining social vulnerability and physical vulnerability to analyse landslide risk at the municipal scale. Geosciences, 8(8), 294.
40. Blaikie, P., Cannon, T., Davis, I., & Wisner, B. (2014). At risk: natural hazards, people's vulnerability and disasters. Routledge.
41. Mahdi, T. W., Hillo, A. N., & Abdul-Sahib, A. A. (2021, March). Development and classification of flood hazard map using 2D hydraulic model. In IOP Conference Series: Materials Science and Engineering (Vol. 1090, No. 1, p. 012122). IOP Publishing.
42. Pérez-Sánchez, J., Senent-Aparicio, J., Segura-Méndez, F., Pulido-Velazquez, D., & Srinivasan, R. (2019). Evaluating hydrological models for deriving water resources in peninsular Spain. Sustainability, 11(10), 2872.